comparable in the level of detail required for safe usage. The hazards of HP do not warrant a preference for LOX.

Conclusions

In this Note, we have compared both the design and operational characteristics of hybrid boosters using the HP/PE and LOX/HTPB propellant combinations. Results of our design study indicate that the HP/PE vehicle is of comparable size and inert weight as the LOX/HTPB system. Primary reasons for this result stem from the inherent simplicity of the HP/PE vehicle and the fact that this system operates at high mixture ratio, thus enabling reduction in fuel chamber and fuel residual mass. In addition, the bulk density advantage enjoyed by the HP/PE system enables a more efficient packaging.

Results of a study of operational characteristics indicate that HP is comparable in both safety and handling risks to LOX. Since the HP/PE engine is inherently simpler in design, we have found that it is also an inherently simpler vehicle to both process and launch. The particular nature of HP offers unique opportunities in system operations, such as auxiliary monopropellant usage, simpler wet leak check capability, and storable propellant operations. The distinct advantages of HP system make it a viable alternative to LOX for an economical strap-on booster.

References

[1]Walter, H., "Experience with the Application of Hydrogen Peroxide for Production of Power," *Jet Propulsion*, Vol. 24, No. 3, 1954, pp. 166–170.

[2]Bloom, R., Davis, N. S., and Levine, S. D., "Hydrogen Peroxide as Propellant," *Journal of the American Rocket Society*, No. 80, March 1950, pp. 3–17.

[3]Andrews, E. G. D., and Mottran, A. W. T., "Trends in the Development of Liquid Propellant Rocket Engines," *Aeronautical Quarterly*, Vol. X, Aug. 1959, pp. 199–210.

[4]Sanz, M. C., "Five-Pound Thrust Liquid Mono-Propellant Rocket," *Journal of the American Rocket Society*, Vol. 25, Sept.–Dec. 1948, pp. 122–125.

[5]Moore, G. E., and Berman, K., "A Solid-Liquid Rocket Propulsion System," *Jet Propulsion*, Nov. 1956, pp. 965–968.

[6]Pugibet, M., and Moutet, H., "Hydrogen Peroxide as an Oxidizer for Hybrid Rocket Engines," NASA TT-F-13034, 1970, p. 2854.

[7]Ventura, M. C., and Heister, S. D., "Hydrogen Peroxide as an Alternative Oxidizer for a Hybrid Rocket Booster," AIAA Paper 93-2411, June 1993.

[8]National Center for Advanced Technologies, "National Rocket Propulsion Strategic Plan," Aerospace Industries Association, Aug. 1990, p. 7.

[9]Byrd, R. J., "Operationally Efficient Propulsion System Study (OEPSS) Data Book, Vol. I—Generic Ground Operations Data," Rocketdyne, Canoga Park, CA, April 14, 1990.

[10]Waldrop, G. S., "Operational Efficient Propulsion System Study (OEPSS) Data Book, Vol. II—Ground Operation Problems," Rocketdyne, Canoga Park, CA, April 24, 1990.

[11]Wong, G. S., "Operational Efficient Propulsion System Study (OEPSS) Data Book, Executive Summary," Rocketdyne, Canoga Park, CA, April 24, 1990.

[12]Guerrero, J., personal communication, Rockwell International Space Systems Div., Downey, CA, June 1993.

[13]Bloom, R., and Brunsvold, N. J., "Anhydrous Hydrogen Peroxide as a Propellant," *Chemical Engineering Progress*, Vol. 53, No. 11, 1957, pp. 541–547.

[14]"Hazards of Chemical Rockets and Propellants Handbook," Vol. 1, General Safety Engineering Design Criteria, NTIS, U.S. Dept. of Commerce, Springfield, VA, May 1972.

[15]"Hazards of Chemical Rockets and Propellants Handbook," Vol. III, Liquid Propellant Handling, Storage, and Transportation, NTIS, U.S. Dept. of Commerce, Springfield, VA, May 1972.

[16]"Hydrogen Peroxide Handbook," Chemical and Material Sciences Dept., Rocketdyne, North American Aviation, Canoga Park, CA, AFRPL-TR-67-144, July 1967.

[17]Krop, Stephen, "The Toxicity and Health Hazards of Rocket Propellants," *Jet Propulsion*, Vol. 24, No. 4, 1954, pp. 223–236.

[18]Schumb, W. C., Sanefield, C. N., and Wentworth, R. L., *Hydrogen Peroxide*, Reinhold, New York, 1955.

[19]"Metals Ignition Study in Gaseous Oxygen (Particle Impact Technique Relating to the Shuttle Main Propulsion System Oxygen Flow Control Valve Tests)," NASA TR-277-001, Johnson Space Center, White Sands Test Facility, 1982.

Effects of the Chemical Reaction Model on Calculations of Supersonic Combustion Flows

Corin Segal,* Hossein Haj-Hariri,† and James C. McDaniel‡
University of Virginia, Charlottesville, Virginia 22901

Introduction

NUMERICAL modeling of reacting supersonic flow in a generic configuration at low enthalpy showed a strong effect of the selection of the reaction model on the solution. The calculation simulated an experiment in which one transverse injector of 1.5 mm diam was located three step heights downstream of a rearward-facing step (the step height is 5 mm). The air inlet conditions were 800 K, a static pressure of $\frac{1}{2}$ atm at Mach 2, with the fuel (gaseous hydrogen) injected at a total temperature of 300 K as an underexpanded jet with a sonic exit. The dynamic pressure ratio of hydrogen-to-air at inlet conditions was 1.5, and the total pressures were 567 and 395 kPa for hydrogen and air, respectively. The resulting overall equivalence ratio was 0.058. The length of the simulated domain was restricted to 4.4 cm (approximately eight step heights downstream of the step) to keep the intensive computational effort at a reasonable level. A mixing, nonreacting calculation was performed to provide a comparison with the reacting case. It required 15 CPU hours, whereas the reacting solution took 33 h to achieve convergence using a Cray-2S. This is effective computer time, which took advantage of the solution technique adopted that artificially accelerated the reactions.

Computational Model

The calculation used the three-dimensional version of SPARK. This code has been used previously in studies of reacting and nonreacting shear layers[1] and in conjunction with combustor experiments, with application to supersonic combustion of hydrogen injected tangentially into a supersonic airstream.[2] Validation studies of mixing were performed for flowfields generated by transverse injection in a Mach 2 stream.[3,4] These works included the evaluation of selected computational techniques, grid resolution, and several algebraic turbulence models. The objective of this work was to test the effects of the chemistry model for low enthalpy supersonic combustion.

The numerical model employs an elliptic three-dimensional Navier-Stokes solver and simulates turbulence based on the

Received March 27, 1992; revision received March 26, 1994; accepted for publication Sept. 5, 1994.

*Graduate Research Assistant, Department of Mechanical and Aerospace Engineering; currently Assistant Professor, University of Florida, Gainesville, FL. Member AIAA.

†Assistant Professor, Department of Mechanical and Aerospace Engineering. Member AIAA.

‡Associate Professor, Department of Mechanical and Aerospace Engineering. Member AIAA.

algebraic model of Baldwin-Lomax, using a fourth-order differenced compact McCormack scheme. The reacting case included the modeling of eight reactions with eight species as described by Eq. (1). The selection of the reaction model and the effects of including the eighth reaction in the model is discussed below:

$$\begin{aligned} H_2 + O_2 &= 2OH \\ H + O_2 &= OH + O \\ OH + H_2 &= H_2O + H \\ O + H_2 &= OH + H \\ 2OH &= H_2O + O \\ H + OH + M &= H_2O + M \\ 2H + M &= H_2 + M \\ H + O_2 + M &= HO_2 + M \end{aligned} \tag{1}$$

Solution Technique

Due to the disparate time scales of chemical kinetics and fluid mechanics the algorithm requires very large computational times to obtain a reacting solution; therefore, the reactions needed to be artificially accelerated in the initial phases of the computation. In addition, due to the low air inlet temperature, autoignition cannot be achieved. During the corresponding experiment, initial steps were taken to ignite the mixture, i.e., the flow was decelerated to subsonic speeds and a source of free radicals was provided by a spark. The ignition technique adopted in the present work was as follows:

1) Initially, the static temperature in all the points of the flowfield was set higher than actual conditions (i.e., uniform T_s = 1000 K).

2) The reacting solution was initiated assuming a velocity distribution in the axial direction closer to the expected combusting solution (i.e., not the solution obtained from the nonreacting study).

3) The chemical kinetics mechanism initially included one reaction only, for which the activation energy was set to zero. Later, the mechanism was changed to include seven and then eight reactions, gradually increasing the activation energy to the correct values.

4) For a very limited number of initial iterations, a small amount of atomic oxygen was added in the jet to accelerate the reactions initiation.

It should be noted that the solution may be sensitive to the initial conditions. This sensitivity is not addressed in this work.

Computational Grid

The computational grid included a 89 × 53 × 21 mesh (approximately 99,000 points), which was considered to be the minimum number of points necessary for a grid-independent solution for this problem. The grid was compressed in the regions of the step, next to the walls and around the jet where large gradients were expected, and at the exit of the domain where extrapolations were used. The domain included a length of approximately nine step heights beginning one step height upstream of the step (hereafter nH is used to denote n times the step height). Because of symmetry, only half of the duct in the spanwise direction was simulated. Previous experiments indicated a significant amount of OH next to the walls; therefore, the walls are expected to have a significant effect on the combustion process, thus the complete width of the duct, including the sidewall boundary layer, was simulated.

Boundary Conditions

The calculations were initiated with a uniform velocity distribution from the throat of the facility's supersonic nozzle to allow boundary-layer growth. In the test section the following boundary conditions were imposed: 1) the input conditions, as derived from the solution for the Mach 2 nozzle; 2) no-slip condition imposed along the duct walls; 3) at the plane of symmetry zero gradients were imposed for all the parameters, except for the spanwise y velocity component, which was set to zero; 4) along the injection wall the temperature recorded during the experiment was prescribed; 5) the other three duct walls were made of uncooled fused silica, they behave almost adiabatically and were modeled as such; 6) at the outflow, the boundary conditions were obtained by linear extrapolation; and 7) the jet was simulated using 48 grid points (semicircle), with a uniform sonic exit profile.

Results

Reacting Solution

Figure 1 shows a plot of the predicted wall pressure distribution compared to the values measured during the experiment. At each cross section the pressure was measured at more than one location. The brackets at the top of the figure indicate the grouping of the pressure taps at each individual streamwise location. The agreement is very good. The absolute pressures are plotted on the left axis with the percent difference on the right axis. The predicted pressures matched the measurements within 5%, with only one exception where the agreement was within 6.7% at pressure port 13. This

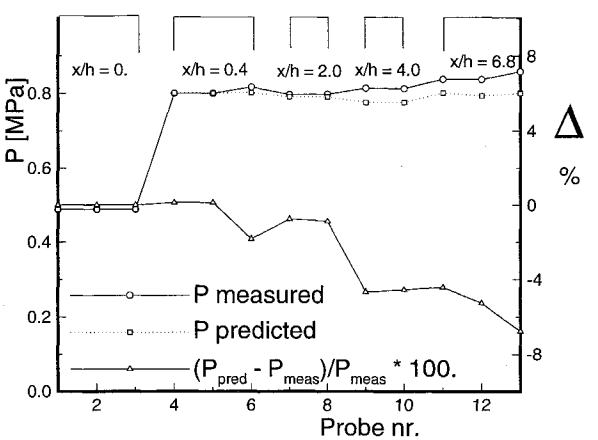

Fig. 1 Wall pressure distribution.

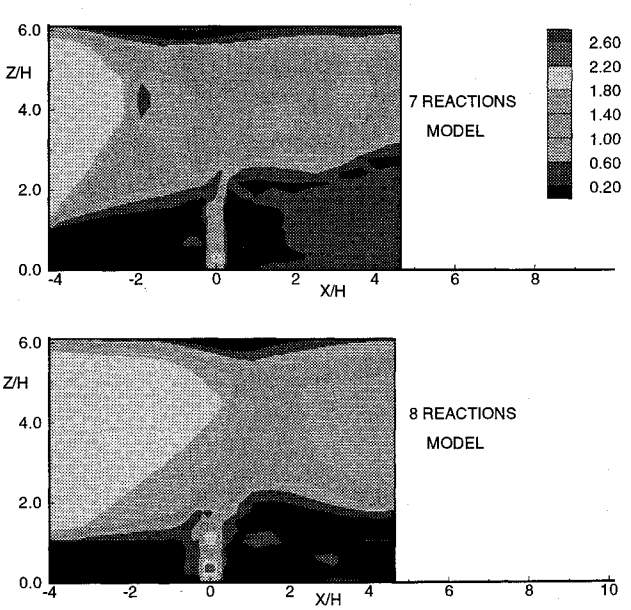

Fig. 2 Effect of chemistry model.

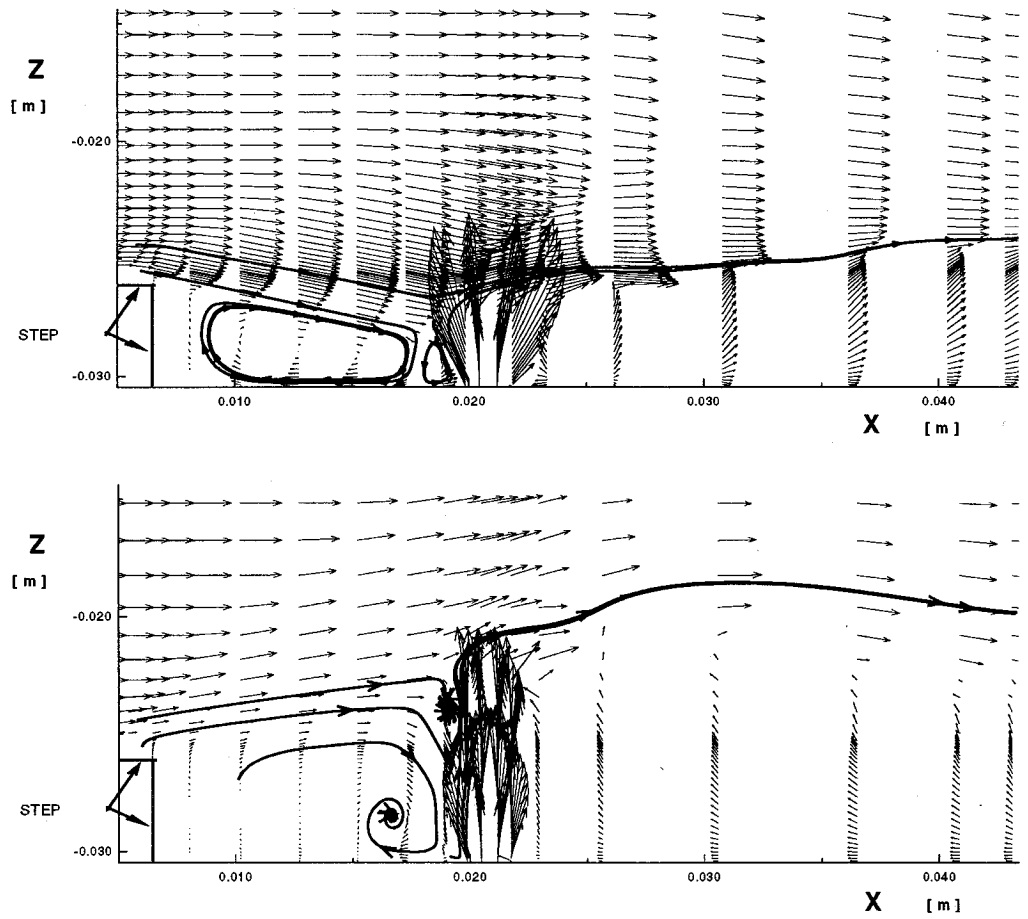

Fig. 3 Velocity distribution in the recirculation region: reacting vs nonreacting case.

pressure port is located on one side of the tunnel that consistently shows (experimentally) higher pressure at every cross section ($\simeq$2%, see $x/h = 0.4$ and $x/h = 6.8$).

Discussion of Reaction Model

The reaction model used in this work is shown by Eq. (1). These reactions were selected from a set of 18 reactions for nine species included at this time in the SPARK code.[5] As described in the solution technique section, the computation was initiated with one reaction with zero activation energy. Then, the model was changed to seven reactions with seven species, similar to the model used in previous work.[2] This model excluded the last reaction in Eq. (1), that of the formation of HO_2. However, HO_2 is a very stable specie at low temperature and acts as a reaction inhibitor, both by depleting the concentration of atomic hydrogen and by absorbing energy from the surrounding gas. Reference 6 includes a detailed theoretical discussion of the effect of this reaction. Since the conditions of the experiment simulated in this calculation were close to thermal choking, the effect of the eighth reaction in the model was particularly strong. Indeed, during the iterations with the seven-reaction model, the calculations indicated that thermal choking occurred: the oblique shock generated at the step became stronger, the pressure constantly increased, and the flow became subsonic in a continuously larger region. Once the eighth reaction, that of formation of HO_2, was implemented, the flow "reaccelerated" back, the upstream interaction disappeared, and the solution marched towards the characteristic supersonic flow bounding the subsonic, reacting region confined near the injection wall. Figure 2 shows a comparison of the Mach distribution in the penetration plane during the process of choking the flow with the seven-reaction model vs the solution obtained after the implementation of the reaction leading to the formation of HO_2. Note that the solution has not reached a steady state in the seven-reaction model case shown in Fig. 2.

Comparison of Nonreacting and Reacting Cases

The configuration of the recirculation region is significantly changed once reactions take place. Figure 3 shows a vector plot comparison of the recirculation and the jet region for the nonreacting and the reacting cases. The flow does not expand around the corner in the reacting case and, in fact, the amount of heat release behind the step is sufficient to cause a shock compression of the main flow immediately behind the step. The clockwise circulation zone is increased in size and the velocity is significantly reduced in magnitude by the chemical reaction. The reacting jet has a completely different structure. In the nonreacting case, the jet has the characteristic barrel shape of an underexpanded jet, ended with a normal shock. Because of the heat release and a reduction in ρu (due to both ρ and u), the jet penetrates significantly deeper into the main flow, approximately 80% more than in the nonreacting situation. The expansion of the fuel jet is also considerably different. Throughout the expansion, an oblique shock wave system is created in the shape of "diamond" cells. This structure is a characteristic of weaker expansions, which is to be expected since the back pressure in the test section with combustion (at the jet plane) is approximately 70% higher than in the nonreacting case.

Acknowledgments

This work was sponsored by NASA Grant NAG 1-795, LaRC, G. B. Northam technical monitor. H. Haj-Hariri acknowledges partial support through this NASA Grant, J. P. Drummond technical monitor.

References

[1]Drummond, J. P., and Hussaini, M. Y., "A Detailed Numerical Model of a Supersonic Reacting Mixing Layer," AIAA Paper 86-1427, June 1986.

[2]Riggins, D. W., and McClinton, C. R., "A Computational Investigation of Flow Losses in a Supersonic Combustor," AIAA Paper 90-2093, July 1990.

[3]Eklund, D. R., Northam, G. B., and Hartfield, R. J., "A Detailed Investigation of Staged Normal Injection into a Mach 2 Flow," 27th JANNAF Combustion Meeting, F. E. Warren Air Force Base, Cheyenne, WY, Nov. 1990.

[4]Eklund, D. R., Northam, G. B., and Fletcher, D. G., "A Validation Study of the SPARK Navier-Stokes Code for Nonreacting Scramjet Combustor Flowfields," AIAA Paper 90-2360, July 1990.

[5]Drummond, G. B., "A Two-Dimensional Numerical Simulation of a Supersonic, Chemically Reacting Mixing Layer," NASA TM 4055, Dec. 1988.

[6]Hitch, B. D., and Senser, D. W., "Reduced H_2-O_2 Mechanisms for Use in Reacting Flow Simulation," AIAA Paper 88-0732, Jan. 1988.

Current Distribution on Isothermal Rod Electrodes in Combustion MHD Generators

Richard P. Heydt*

SRI International, Menlo Park, California 94025

Introduction

ELECTRODE geometry influences MHD generator performance and strongly affects current distribution. This Note summarizes measurements of current distribution made on rod-shaped electrodes in the Stanford M-2 MHD generator. The measurements reported here are several years old, but remain unique for combustion MHD power generation.

In segmented-Faraday generators, with flat, flush-mounted electrodes, current concentrates at the upstream edges of anodes and downstream edges of cathodes, because the axial electric field created by segmentation is locally shorted at the electrode surface. Current concentrations enhance electrode surface erosion and play a major role in interelectrode, axial-field breakdown, through direct heating of the electrode-insulator interface and local heating of the plasma at the electrode surface.

These problems may be alleviated if flat electrodes are replaced with transverse rod electrodes, raised slightly off the generator electrode wall. The rod geometry may be especially useful in suppressing insulator-breakdown arcs, as rod electrodes and interelectrode insulators are in contact in only a small region along the generator sidewall. Since there are no insulator-electrode edges perpendicular to the flow direction, rods can also eliminate concentrations, while distributing current over a larger total area.

Rod electrodes have been studied computationally[1] and experimentally[2] in nonequilibrium generators. No experimental measurements of current distribution have been reported for either combustion or nonequilibrium generators.

The purpose of this research was to determine how load current is distributed on a rod electrode in a combustion MHD generator. It is important to distinguish between the effects of geometry and temperature variations along the electrode circumference, particularly when the plasma flowfield is complex, as with an array of rods. The experimental intent was to produce a near-isothermal rod surface, so that the measured current distributions would primarily represent the effect of electrode shape.

Measurement results are presented in this Note along with predictions from a current-distribution model.

Received Jan. 21, 1994; revision received Sept. 12, 1994; accepted for publication Oct. 3, 1994.

*Research Engineer.

Experiment Description

The experiments were run in the M-2 facility at Stanford University. The fuel was ethanol-seeded with potassium hydroxide, and was burned in oxygen, with nitrogen added as diluent.

Figure 1 illustrates the layout and dimensions of the MHD test section. There were 13 electrode pairs, with the bottom electrode of each pair being a rod. For experimental practicality, the rods were artificially large (a realistic rod-diameter-to-channel-height ratio might be 0.01 or 0.02). One of the rod electrodes was divided into eight segments for current-distribution measurement. Each segment had independent surface-temperature control.

The current distributions reported here are applied-field measurements. Voltage was applied across the top, flat electrode and the bottom, segmented-rod electrode in the presence of magnetic field and plasma flow. Each distribution represents an average of two to five measurements. Current density was kept low to maintain diffuse transfer at the electrode surface. Table 1 gives approximate values of experimental parameters.

Current-Distribution Model

A diffuse-transport, current-distribution model was developed to evaluate the experimental results. The model[3] is based on the two-dimensional, steady-state MHD electrical and energy equations, which were solved by finite difference. A crucial issue is that the current flow pattern is highly dependent on the spatial variation of plasma conductivity, and thus

Table 1 Nominal experiment parameters

Magnetic flux density	2.5 T
Plasma flow velocity	250 m/s
Plasma temperature	2650 K
Rod segment surface temperatures	800 K ± 50 K
Applied (Faraday) voltage	100–200 V
Rod surface current density	0.1–0.3 A/cm^2

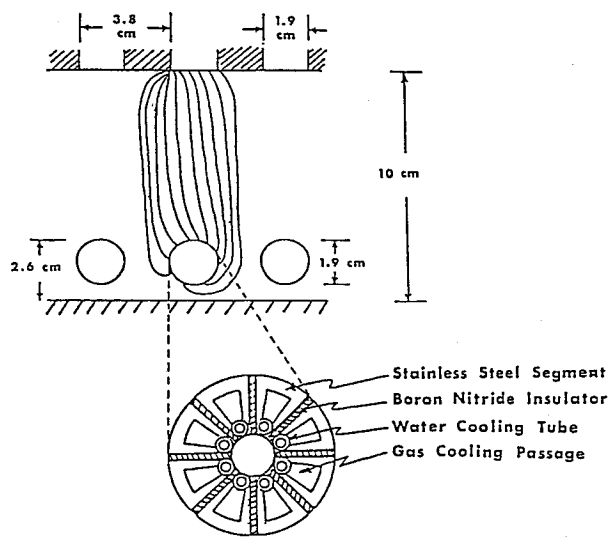

Fig. 1 Side view of the M-2 channel, showing dimensions and a cross section of the segmented rod electrode.